Synthesis, characterization, anti-corrosion behavior and theoretical study of the new organic dye: 3-oxo-3*H*-spiro[isobenzofuran-1,9´-xanthene]-3´,6´-diyl bis(3-methyl-benzenesulfonate)

N. Arrousse,[1] El. Mabrouk,[1,2] B. Hammouti,[3]* F. El Hajjaji,[1]* Z. Rais[1] and M. Taleb[1]

[1]*Engineering Laboratory of organometallic, Molecular Materials and Environment, Faculty of science, University Sidi Mohamed Ben Abdellah, Fez, Morocco*
[2]*Departement of Chemistry, Faculty of Science and Technics, BP 509 Boutalamine, Errachidia, Moulay Ismail University Meknes, Morocco*
[3]*Mohammed Premier University, LCAE, Faculty of science, 60000 Oujda, Morocco*
E-mail: hammoutib@gmail.com, el.hajjajifadoua25@gmail.com

Abstract

The present work covers the recent synthetic of 3-oxo-3*H*-spiro[isobenzofuran-1,9´-xanthene]-3´,6´-diyl bis (3-methylbenzenesulfonate) in high yield attain 91% through reaction between fluorescein and 4-methylbenzenesulfonyl chloride for 8 hours under different operating conditions. We have developed an environmentally friendly compound, mild condition protocol and convenient procedure for the preparation of this xanthene derivative. The structure of the new organic dye was determined by spectroscopic methods such as: ^{1}H NMR, ^{13}C NMR, infrared and MS data. This reaction has been studied also theoretically using Gaussian 09 software based on the DFT method at B3LYP/6-31G(d,p), in order to explain the possibility of these reaction through the quantum chemical parameters. The results obtained theoretically are in good correlation with those obtained experimentally. The inhibition effect of 3-oxo-3*H*-spiro[isobenzofuran-1,9´-xanthene]-3´,6´-diyl bis(3-methyl-benzenesulfonate (NAR1) on the corrosion of mild steel in molar hydrochloric acid solution. The experimental part was performed by studying the stability of the synthetic product in the corrosive medium and the inhibition behavior was investigated using absorbance difference measurements; the result indicates that NAR1 is a good inhibitor in acidic medium at low concentration at 1 ppm, the percentage of inhibition efficiency achieves 93%. The surface analysis of mild steel was investigated using scanning electron microscopy (SEM) and Energy dispersive X-ray (EDX) methods and show the adsorption behavior of inhibitor on the surface of mild steel.

Keywords: *new organic dye, xanthene derivative, inhibitor, DFT/B3LYP method with the 6-31G base (d,p), absorbance, MEB/EDX.*

Received: March 21, 2020. Published: May 25, 2020 doi: 10.17675/2305-6894-2020-9-2-18

1. Introduction

The synthesis of new compounds containing heterocyclic systems occupies an important place in the realm of synthetic organic chemistry [1–6]. They exhibit several applications in medicinal chemistry [10, 11] and they constitute an essential pharmacophore in many naturally occurring and biologically active agents [12–16].

Fluorescence typically occurs in aromatic molecules and heterocycles, called fluorophores or fluorescent dyes. Fluorescent molecules always contain a chromophore, the part of a molecule responsible for its color. Chromophores usually appear in conjugated π-systems and metal complexes. These endogenous fluorophores are responsible for autofluorescence of biological structures such as mitochondria or lysosomes [17]. Polycyclic aromatic compounds represent a class of fluorescent dyes widely applied as useful synthetic biomolecule labels [18–29]. Fluorescent dyes, which contain a xanthene, three-membered ring structure in their molecules, are known as xanthene dyes. Xanthenes are structurally related to xanthones, which represent the central core of many naturally occurring compounds. Derivatives of xanthones exhibit diverse pharmacological activities. The biological activities of synthetic and naturally occurring xanthone derivatives depends on the various substituents and their position [30, 31]. 3,6-Dihydroxyxanthenone and its derivatives can be used as building blocks in the synthesis of new xanthene dyes such as Tokyo Green. In 1871 the German chemist, Nobel prize laureate, discoverer of plant dye indigo Adolf von Baeyer [32] investigated the synthesis of phenolphthalein by condensation of phthalic anhydride with phenol under acidic conditions. That same year performed the $ZnCl_2$-catalyzed synthesis of resorcinophthalein from phthalic anhydride and 1,3-dihydroxybenzene, known as resorcinol [33]. This compound was assigned as fluorescein. Despite its antiquity, fluorescein remains one of the most widely utilized xanthene fluorophores in modern biochemical, biological and medicinal research. Following the research done on the synthesis of new fluorescein derivatives and in the synthesis of heterocyclic systems of xanthene derivatives, we focused in this work on the synthesis of 3-oxo-3*H*-spiro[isobenzofuran-1,9′-xanthene]-3′,6′-diyl bis(3-methylbenzene-sulfonate) with the aim to have access to new active biomolecule with a very good yield. Then, the anti-corrosion behavior of synthetic compound has been studied using difference absorbance method and the surface of mild steel analysis using MEB/EDX technical.

2. Results and discussions of the synthesis reaction

Our strategy is based on the *O*-tosylation of 4-methylbenzenesulfonyl chloride **2** with fluorescein **1** (Scheme 1). As a first step and to optimize the different reaction conditions (choice of base, solvent ...), we conducted several test reactions. For all these tests, the reactions were followed by TLC and ^{1}H NMR. The Infrared spectroscopic studies show the bands confirming the presence of the groups C=O, C–O, S=O, $–CH_3$, and =CH. Yields are given as pure product after recrystallization from acetone/methanol.

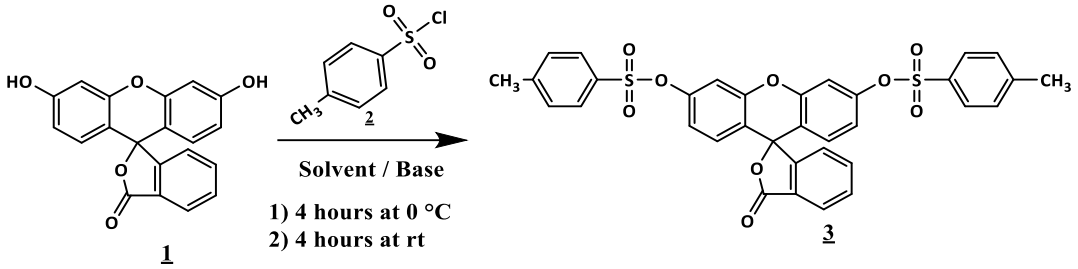

Scheme 1. *O*-tosylation of 4-methylbenzenesulfonyl chloride **2** with fluorescein **1**.

The *O*-tosylation reaction was carried out in different solvents (DCM, acetone, CH_3CN and THF) for 4 hours at 0°C in the presence of various bases (Et_3N, pyridine or DIEPA). The product 3 synthesized with satisfactory yields was characterized by nuclear magnetic resonance, Infrared and mass spectrometry. The results are summarized in Table 1.

Table 1. Optimization of reaction conditions.

Reaction conditions	**– DCM**	**– THF**	**NaOH THF**	**NaOH Acetone**	**Pyridine Acetone**	**Et_3N Acetone**	**DIEPA DCM**	**DIEPA CH_3CN**	**DIEPA Acetone**
Yield (%)	0	0	40	62	70	80	42.5	88	91
Reaction Time (h)	8 hours								

DCM is dichloromethane, CH_3CN is acetonitrile, THF is tetrahydrofuran, Et_3N is triethylamine, and DIEPA is diisopropylethylamine.

In summary, after several attempts of reactions without a base or in the presence of bases such as triethylamine, pyridine and diisopropylethylamine, reaction with diisopropylethylamine (DIEPA) in dry acetone give the best results. The solvents played an important role in the substitution of fluorescein. Further studies established that absolute acetone also was the best choice among the solvents (DCM, acetone, CH_3CN and THF) screened (Table 1). All reactions that were conducted in DCM or THF had low yields.

As shown in Scheme 1, the *O*-tosylation of 4-methylbenzenesulfonyl chloride **2** with fluorescein 1 leads to the product 3-oxo-3*H*-spiro[isobenzofuran-1,9′-xanthene]-3′,6′-diyl bis(3-methylbenzenesulfonate) **3** with an excellent chemical yield. This reaction was carried out in dry acetone for 4 hours at 0°C in addition to 4 hours at room temperature in the presence of diisopropylethylamine and was determined by usual spectroscopic techniques, such as ^{1}H-NMR, ^{13}C-NMR, Infrared and MS.

3. Experimental Section

3.1. General

Melting points were determined with an electrothermal melting point apparatus and are uncorrected. NMR spectra (^{1}H, ^{13}C) were recorded on a Bruker AM 300 (operating at

300.13 MHz for ^{1}H, at 75.47 MHz for ^{13}C) spectrometer (Regional University Center of Interface, Fez). NMR data are listed in ppm and are reported relative to tetramethylsilane (^{1}H, ^{13}C); residual solvent peaks being used as internal standard. All reactions were followed by TLC. TLC analyses were carried out on 0.25 mm thick precoated silica gel plates (Merck Fertigplatten Kieselgel 60F254) and spots were visualized under UV light or by exposure to vaporized iodine. Mass spectra were recorded on a Polaris Q Ion Trap GC/MS Mass Spectrometer (Regional University Center of Interface, Fez).

3.2. Typical procedure for O-tosylation

To a stirring solution of fluorescein (0.34 g, 1 mmol) in 5 mL of solvent cooled to 0°C was added 1.1 mmol of base; 4-toluenesulfonyl chloride (0.8 g, 4 mmol, 4.0 equiv) in 3 mL of solvent was added dropwise over 2 h with continuous cooling. The solution was cooled additional 2 h. TLC monitored the mixture on silica gel (ether/hexane, 80:20). After 4 hours, the conversion of the starting material was complete and a new product was noticed. The solvent was evaporated under reduced pressure. The residue was quenched with saturated aqueous solution of ammonium chloride (20 mL) and extracted with dichloromethane (20 mL×3). The organic phase was dried on sodium sulfate (Na_2SO_4) and the solvent was removed under reduced pressure. The product was purified by twice recrystallization from acetone/methanol. The product was obtained as a white solid with the good yield.

3.3. 3-Oxo-3H-spiro[isobenzofuran-1,9′-xanthene]-3′,6′-diyl bis(3-methylbenzenesulfonate) ***3***

Yield = 91%; Melting point (ether/hexane): 172–174°C; R_f = 0.8 (ether). ^{1}H NMR (Bruker, 300.13 MHz, $CDCl_3$): δ (ppm) = 2.48 (s, 6H, CH_3), 6.68–6.76 (m, 4H, H_{arom}), 7.03 (d, 2H, H_{arom}), 7.13–7.15 (m, 1H, H_{arom}), 7.36 (d, 4H, H_{arom}), 7.63–7.77 (m, 6H, H_{arom}), 8.02–8.04 (m, 1H, H_{arom}). ^{13}C NMR (75.47 MHz; $CDCl_3$): δ (ppm) = 168.3 (C=O), 152, 150.5 (2C), 150.1 (2C), 146.1 (2C), 136.1, 131.2 (2C) 130.5 (4C), 130.0 (2C), 128.3 (4C), 126.4, 125.0 (2C), 124.0, 118.5 (2C), 117.6 (2C), 110.7 (2C), 81.05 (C1), 79.7, 21.81 (2C, C-9′, C-10′). MS-EI: ($[M+H]^+$, 100%) 641.6; $C_{34}H_{24}O_9S_2$. FT-IR (KBr, cm^{-1}): 3099 ν (=C–H, aromatic), 1750 ν (C=O, lactone), 1596 ν (C=C, arom.), 1491, 1432, 1371 ν (S=O), 1235, 1142, 1092.

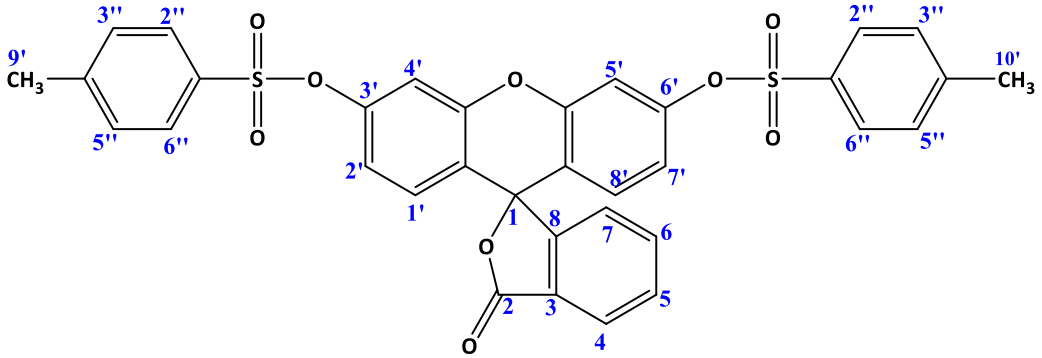

4. Theoretical study of the synthesis reaction

4.1. Calculation methodology

In this work, we used:

- The DFT/B3LYP density functional theory method with the 6-31G base (d,p) for quantum calculations.
- The GaussView 5.0 program for the construction, visualization of molecular models and the visualization of geometries.
- The GAUSSIAN 09 program for the optimization of equilibrium geometries.
- Natural Population Analysis (NPA) for calculating local indices of the reactivity.
- The MARVINSKETCH program to determine the distribution of different forms of fluorescein with pH.

4.2. Results and Discussion

4.2.1. Justification for choosing the DFT/B3LYP method

In order to justify the choice of the DFT/B3LYP calculation method used in the rest of this work, it is necessary to make a comparison between the main calculation methods implemented in the Gaussian 09 software.

In addition to the DFT/B3LYP method with the 6-31G base (d,p), we have chosen two others: semi-empirical (MP2/6-31G(d,p)) and Hartree-Fock (HF/6-31G(d,p)), the calculations are applied for the reagents of the reaction studied.

4.2.1.1. Comparison of interatomic distances

From the results of Table 2 we find that the DFT/6-31G(d,p) method gives interatomic distances closer to the real values.

Table 2. Interatomic distances of fluorescein (R1) and tosyl chloride (R2) found after optimization by the methods DFT/6-31G(d,p), HF/6-31G(d,p) and MP2/6-31G(d,p).

Reagents / Geometry	**Interatomic distances / Calculation methods**		
	DFT/6-31G(d,p)	**HF/6-31G(d,p)**	**MP2/6-31G(d,p)**
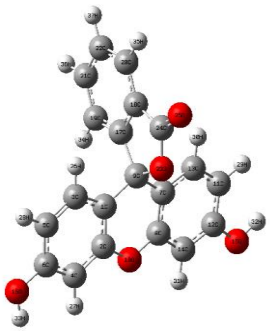 R1	$dC_1–C_2=1.396$	$dC_1–C_2=1.394$	$dC_1–C_2=1.389$
	$dC_1–C_3=1.405$	$dC_1–C_3=1.407$	$dC_1–C_3=1.408$
	$dC_3–H_{26}=1.085$	$dC_3–H_{26}=1.082$	$dC_3–H_{26}=1.084$
	$dC_3=C_5=1.384$	$dC_3=C_5=1.388$	$dC_3=C_5=1.389$
	$dC_5–C_6=1.404$	$dC_5–C_6=1.407$	$dC_5–C_6=1.409$
	$dC_6–O_{16}=1.362$	$dC_6–O_{16}=1.363$	$dC_6–O_{16}=1.365$
	$dO_{16}–H_{33}=0.966$	$dO_{16}–H_{33}=0.950$	$dO_{16}–H_{33}=0.972$

Reagents / Geometry	Interatomic distances / Calculation methods		
	DFT/6-31G(d,p)	**HF/6-31G(d,p)**	**MP2/6-31G(d,p)**
	$dC_2–O_{10}=1.369$	$dC_2–O_{10}=1.371$	$dC_2–O_{10}=1.372$
	$dC_{24}=O_{25}=1.206$	$dC_{24}=O_{25}=1.205$	$dC_{24}=O_{25}=1.207$
	$dC_{18}–C_{24}=1.482$	$dC_{18}–C_{24}=1.480$	$dC_{18}–C_{24}=1.482$
	$dC_9–C_{17}=1.523$	$dC_9–C_{17}=1.527$	$dC_9–C_{17}=1.528$
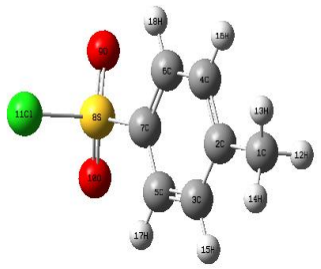 R2	$dC_1–H_{12}=1.093$	$dC_1–H_{12}=1.094$	$dC_1–H_{12}=1.097$
	$dC_1–C_2=1.508$	$dC_1–C_3=1.505$	$dC_1–C_3=1.506$
	$dC_2=C_4=1.403$	$dC_2=C_4=1.404$	$dC_2=C_4=1.403$
	$dC_3–H_{15}=1.086$	$dC_3–H_{15}=1.085$	$dC_3–H_{15}=1.087$
	$dC_3=C_5=1.391$	$dC_3=C_5=1.389$	$dC_3=C_5=1.385$
	$dC_5–C_7=1.395$	$dC_1–C_2=1.390$	$dC_1–C_2=1.392$
	$dC_7=C_8=1.394$	$dC_7=C_8=1.395$	$dC_7=C_8=1.394$
	$dC_7–S=1.782$	$dC_7–S_8=1.784$	$dC_7–S_8=1.787$
	$dS–Cl=2.140$	$dS–Cl=2.141$	$dS–Cl=2.142$
	$dS=O=1.457$	$dS=O=1.455$	$dS=O=1.456$

4.2.1.2. Comparison of calculation time

Time is money. For this reason, we always try to perform efficient calculations but in the shortest time possible, for this reason the time factor remains among the most important factors in the choice of the calculation method. The optimization time in seconds of each of the two reagents for each method is represented in the form of a diagram.

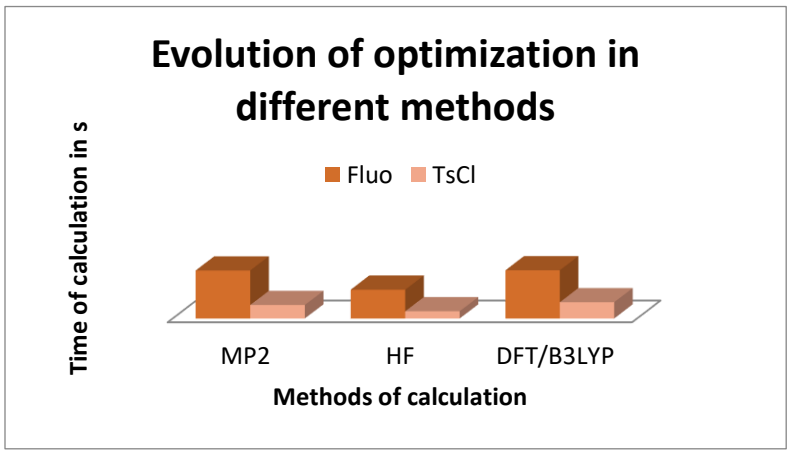

Figure 1. Evolution of time of optimization of the two reagents TsCl (4-methylbenzenesulfonyl chloride or Tosyl chloride) and FLUO (Fluorescein) in second for the methods: DFT / B3LYP, MP2, HF.

From Figure 1 it can be seen that the method that gives the calculation results in the minimum possible time is the HF method, while the other two methods: DFT and MP2 give the results with a longer time.

4.2.1.3. Comparison of the total energy given by each method

In order to confirm the most powerful method, one must also take into account the total energy obtained by each method for the two reagents.

Table 3 represents the total eV energy values of fluorescein and tosyl chloride given by DFT, MP2, and HF.

Table 3. E_{total} eV fluorescein and tosyl chloride for DFT, MP2, and HF methods.

Energy (eV)	MP2	HF	DFT
R1	–31167.5256	–31169.7081	–31171.2957
R2	–1279.7534	–1281.5123	–1282.2354

From the results in Table 3, the lowest total energy for both reagents is given by the DFT method.

In conclusion, the DFT method makes it possible, after optimization, to obtain interatomic distances that are closer than those of reality; also the lowest total energy values and with a reasonable calculation times hence the justification for our choice of the DFT as a calculation method in the present work.

4.2.2. Optimization of interatomic distances and determination of the density of charges and the angles of the reagents

The optimized structures allow direct access to all the parameters related to the geometry of the molecules, namely: the densities of charges, the interatomic distances, the angles ... All our calculations were performed by the DFT/B3LYP density functional theory method, with the base 6-31G(d,p). The values of these quantities are collated in Tables 4 and 5. The optimized reagent geometries are respectively shown in Figures 2 and 3.

Table 4. Density of charge of the atoms of the two reagents.

Fluorescein (R1)		Tosyl chloride (R2)	
C_1; C_7	0.11	C_1	–0.38
C_2; C_8	0.28	C_2	0.12
C_3; C_{11}; C_{13}	–0.14	C_3	–0.12
C_4	–0.19	C_4	–0.12
C_5; C_{19}	–0.12	C_5	–0.06
C_6; C_{12}	0.33	C_6	–0.06

C_9	0.06	C_7	–0.18
O_{15}; O_{16}	–0.57	S_8	1.00
O_{18}	–0.56	O_9	–0.48
O_{23}	–0.50	O_{10}	–0.48
O_{25}	–0.51	Cl_{11}	–0.18

Table 5. Interatomic distances and angles corresponding to reagents.

Reagents	Distance Å	Angle °
R1	$dC_1–C_2 = 1.396$ $dC_1–C_3 = 1.405$ $dC_3–H_{26} = 1.085$ $dC_3 = C_5 = 1.384$ $dC_5–C_6 = 1.404$ $dC_6–O_{16} = 1.362$ $dO_{16}–H_{33} = 0.966$ $dC_2–O_{10} = 1.369$ $dC_{24} = O_{25} = 1.206$ $dC_{18}–C_{24} = 1.482$ $dC_9–C_{17} = 1.523$	$A(C_1,C_2,C_3) = 31.305°$ $A(C_3,C_4,C_5) = 120.038°$ $A(O_{16},C_6,C_5) = 117.201°$ $A(O_{23},C_{24},O_{25}) = 122.190°$
R2	$dC_1–H_{12} = 1.093$ $dC_1–C_2 = 1.508$ $dC_2 = C_4 = 1.403$ $dC_3–H_{15} = 1.086$ $dC_3 = C_5 = 1.391$ $dC_5–C_7 = 1.395$	$A(C_1,C_2,C_3) = 120.668°$ $A(C_2,C_3,C_5) = 121.263°$ $A(C_7,S_8,O_9) = 110.340°$ $A(C_7,S_8,Cl_{11}) = 102.521°$

Figure 2. Fluorescein structure optimized by the DFT method B3LYP/6-31G(d,p).

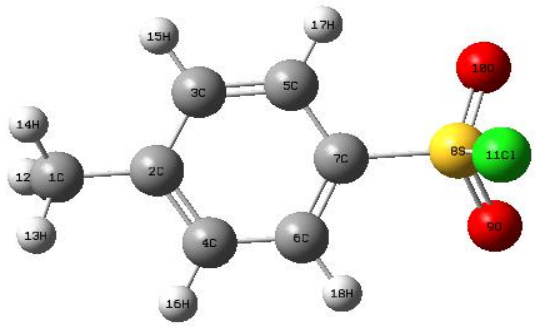

Figure 3. Structure of 4-toluenesulfonyl chloride optimized by the DFT method B3LYP/6-31G(d,p).

4.2.3. Theoretical study of the condensation reaction of fluorescein (R1) and tosyl chloride (R2)

4.2.3.1. Thermodynamic study

We have gathered some thermodynamic quantities characterizing of the reaction between of R1 on R2 in Table 6.

Table 6. Thermodynamic quantities characterizing the reaction of fluorescein R1 and tosyl chloride R2 calculated by DFT/B3LYP 6-31G(d,p).

Thermodynamic quantities of the reaction	
ΔH (Kcal/mole)	–36.4566
ΔS (Kcal/mole·K)	–0.0260
ΔG (Kcal/mole)	–28.6913

The enthalpy value of the ΔH_r reaction is negative, hence the exothermic nature of this reaction.

The free enthalpy variation ΔG_r that corresponds to the condensation reaction is negative; therefore, this reaction is possible and favored thermodynamically.

4.2.3.2. Prediction of electrophile/nucleophilic character of reagents

In order to highlight the electrophilic/nucleophilic nature of the reagents we calculated:

– The HOMO/LUMO energy gaps of the reaction, and the HOMO and LUMO molecular orbital energies of each reagent.
– The gap energies ΔE, the electronic chemical potentials μ, the chemical hardness η, the global electrophilic indices ω, the global nucleophilic indices N, by the following equations [34]:

$$\Delta E(\mathrm{I}) = E_{\mathrm{HOMO}}\ (\mathrm{fluo}) - E_{\mathrm{LUMO}}\ (\mathrm{TsCl})$$

$$\Delta E(\mathrm{II}) = E_{\mathrm{HOMO}}\ (\mathrm{TsCl}) - E_{\mathrm{LUMO}}\ (\mathrm{fluo})$$

$$\omega = \mu^2/2\cdot\eta$$

$$\mu = (E_{\mathrm{HOMO}} + E_{\mathrm{LUMO}})/2$$

$$\eta = E_{\mathrm{LUMO}} - E_{\mathrm{HOMO}}$$

$$N = E_{\mathrm{HOMO}} - E_{\mathrm{HOMO}}\ (\mathrm{TCE})$$

With E_{HOMO} (TCE) = –9.3686 eV calculated by DFT/B3LYP 6-31G(d,p).

The results from Table 7 and Figure 4 show that the gaps $|E_{\mathrm{HOMO}}$ (R1)$-E_{\mathrm{LUMO}}$ (R2)|, of the order of 3.5241 eV, are energetically weaker than the gaps $|E_{\mathrm{HOMO}}$ (R2)$-E_{\mathrm{LUMO}}$ (R1)| which are of the order of 5.9903 eV, which shows that the tosyl chloride (R2) has an electrophilic character while the fluorescein (R1) behave like a nucleophile.

Table 7. HOMO and LUMO energies, and the energy differences between the two possible HOMO/LUMO combinations of the reagents by the DFT/B3LYP method in the base (6-31G)(d,p).

Compound	*E* (eV)	HOMO (eV)	LUMO (eV)	Δ*E* (I) (eV)	Δ*E* (II) (eV)
R1	–31171.2957	–6.1304	–1.4367		
R2	–34823.7870	–7.4270	–2.6063	–3.5241	–5.9903

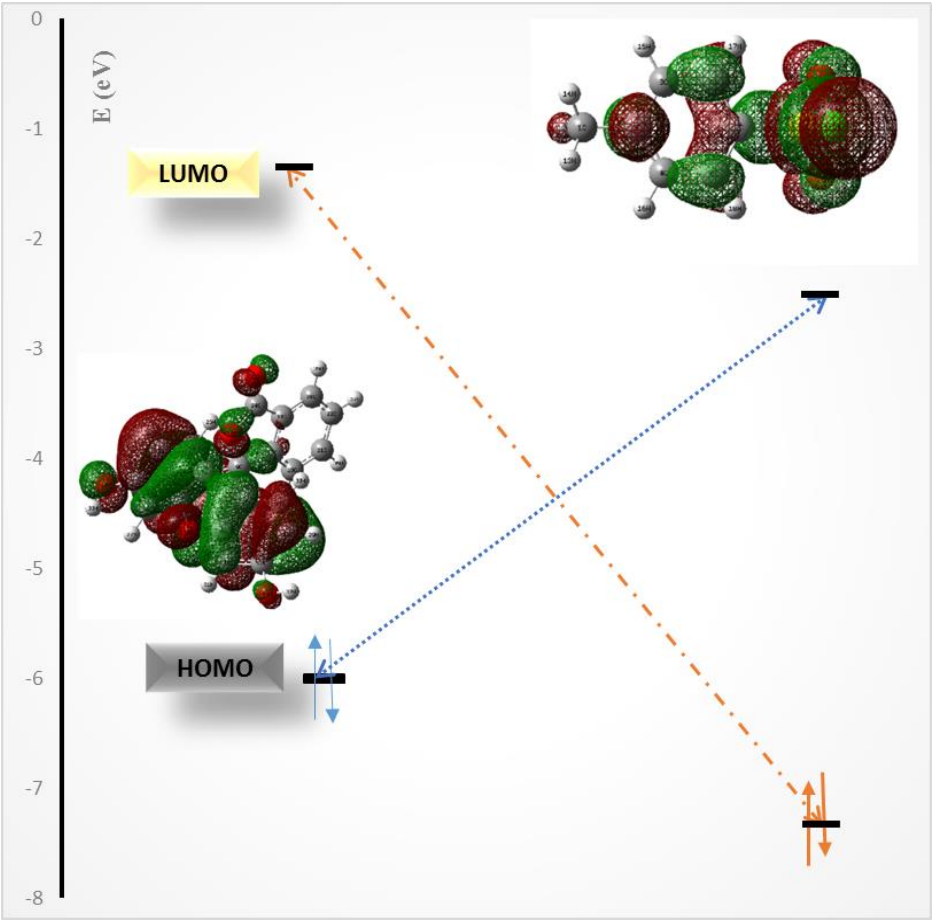

Figure 4. HOMO and LUMO energy diagram of reagents.

4.2.3.3. Theoretical analysis of reagents by global properties

Table 8. Electronic chemical potential μ, chemical hardness η, global electrophilicity ω, global nucleophilicity *N*, B3LYP DFT/6-31G(d,p).

Compound	*E* (eV)	μ (eV)	η (eV)	S(I) (eV)	ω (eV)	*N* (eV)
R1	–31171.2957	–2.3468	4.6937	0.1065	0.5867	2.9881
R2	–34823.7870	–2.4104	4.8208	0.1037	0.6026	1.6915

Table 8 shows that the electronic chemical potential μ of fluorescein (μ = –2.3468 eV) is on a level of energy higher than that of tosyl chloride (μ = –2.4104 eV), which implies that electron transfer takes place from fluorescein to tosyl chloride. The global nucleophilicity *N* of fluorescein (*N* = 2.9881 eV) is significantly higher than that of tosyl chloride (*N* = 1.6915 eV), which means that fluorescein plays the role of a nucleophile whereas TsCl is an electrophile. The same conclusion can be drawn from the values of the global electrophilicity ω. Chemical hardness of fluorescein (η = 4.6937 eV) is less than that of tosyl chloride (η = 4.8208 eV), which means that fluorescein retains few electrons in its environment, unlike tosyl chloride, which maintains them in its own environment, and consequently the transfer of electrons takes place from fluorescein to tosyl chloride.

In conclusion, HOMO/LUMO gap calculations, electronic chemical potentials and global electrophilicity and nucleophilicity indices show globally the nucleophilic nature of fluorescein and the electrophilic character of tosyl chloride.

4.2.3.4. Prediction of local reactivity of reagents

• *Application of the Domingo polar model, using Fukui indices* f_k^+ *and* f_k^-

According to Domingo's polar model, the static indices of local electrophilicity ω_k and local nucleophilicity N_k are reliable descriptors for the prediction of the most favored electrophilic-nucleophilic interaction for the formation of a chemical bond between two atoms. It occurs between the most electrophilic site (characterized by the highest value of ω_k) of the electrophilic molecule and the most nucleophilic site (characterized by the highest N_k value) of the nucleophilic molecule. The local electrophilic values ω_k for the reactive atoms and the local nucleophilic N_k of the tosyl chloride and fluorescein atoms calculated from the natural NPA populations by the DFT/B3LYP 6-31G(d,p) method are reported in Tables 9 and 10.

$$\omega_k = \omega \cdot f_k^+ \ (\omega = 0.6026 \text{ eV}) \text{ and } N_k = N \cdot f_k^- \ (N = 2.9881 \text{ eV}).$$

$$f_k^+ = [P_k(N+1) - P_k(N)] \text{ for a nucleophilic attack.}$$

$$f_k^- = [P_k(N) - P_k(N-1)] \text{ for an electrophilic attack.}$$

Table 9. Natural populations of reagents calculated by the DFT/B3LYP 6-31G method (d,p).

Natural populations					
Fluorescein			**TsCl**		
Atoms	***P*(*N*)**	***P*(*N*−1)**	**Atoms**	***P*(*N*)**	***P*(*N*+1)**
C_1	6.15300	6.05094	C_1	6.71022	6.69984
C_2	5.65370	5.61948	C_2	5.98321	6.05961
C_3	6.18664	6.18842	C_3	6.22547	6.23668
C_4	6.35306	6.32610	C_4	6.22523	6.23659
C_5	6.30583	6.17120	C_5	6.19874	6.25263
C_6	5.65439	5.63749	C_6	6.19892	6.25242
C_7	6.15164	6.07941	C_7	6.35084	6.36044
C_8	5.6562	5.63102	S_8	13.87483	14.03983
C_9	5.74195	5.75232	O_9	8.88976	8.99649
O_{10}	8.48562	8.36704	O_{10}	8.88977	8.99649
C_{11}	6.32575	6.21142			
C_{12}	5.65537	5.64789			
C_{13}	6.18392	6.17839			
C_{14}	6.33306	6.29615			
O_{15}	8.69874	8.67317			
O_{16}	8.69839	8.66215			
C_{17}	6.01968	6.03323			
C_{18}	6.1753	6.1694			
C_{19}	6.22323	6.21679			
C_{20}	6.19041	6.18343			
C_{21}	6.20644	6.19872			
C_{22}	6.23717	6.22533			
O_{23}	8.54861	8.53162			
C_{24}	5.17982	5.17612			
O_{25}	8.61000	8.58076			

Table 10. Fukui indices (f_k^+ and f_k^-) and local electrophilicity values ω_k for reactive TsCl atoms and N_k local nucleophilicity for reactive fluorescein atoms calculated by NPA natural population analysis.

Local indices NPA					
Fluorescein			**TsCl**		
Atoms	f_k^-	N_k	**Atoms**	f_k^+	ω_k
C_1	0.102	0.305	C_1	–0.010	–0.006
C_2	0.034	0.102	C_2	0.076	0.046
C_3	–0.002	–0.005	C_3	0.011	0.007
C_4	0.027	0.081	C_4	0.011	0.007
C_5	0.135	0.402	C_5	0.054	0.032
C_6	0.017	0.050	C_6	0.053	0.032
C_7	0.072	0.216	C_7	0.010	0.006
C_8	0.025	0.075	S_8	0.165	0.099
C_9	–0.010	–0.031	O_9	0.107	0.064
O_{10}	0.119	0.354	O_{10}	0.107	0.064
C_{11}	0.114	0.342			
C_{12}	0.007	0.022			
C_{13}	0.006	0.017			
C_{14}	0.037	0.110			
O_{15}	0.026	0.076			
O_{16}	0.036	0.108			
C_{17}	–0.014	–0.040			
C_{18}	0.006	0.018			
C_{19}	0.006	0.019			
C_{20}	0.007	0.021			
C_{21}	0.008	0.023			
C_{22}	0.012	0.035			
O_{23}	0.017	0.051			
C_{24}	0.004	0.011			
O_{25}	0.029	0.087			

From where [35]:

$P_k(N)$: electron population of the atom k in the neutral molecule.
$P_k(N+1)$: electron population of the k atom in the anionic molecule.
$P_k(N-1)$: electron population of the k atom in the cationic molecule.

The results found are not in agreement with those desired in the synthesis, as the values of the Fukui indices are low in the O_{15} and O_{16} sites. This indicates that the neutral form of fluorescein does not give a good approach to the reaction, hence the need to work with a base in order to extract the two protons from the fluorescein diols. pH remains, moreover, a parameter to be determined to lead to this reactive form of fluorescein.

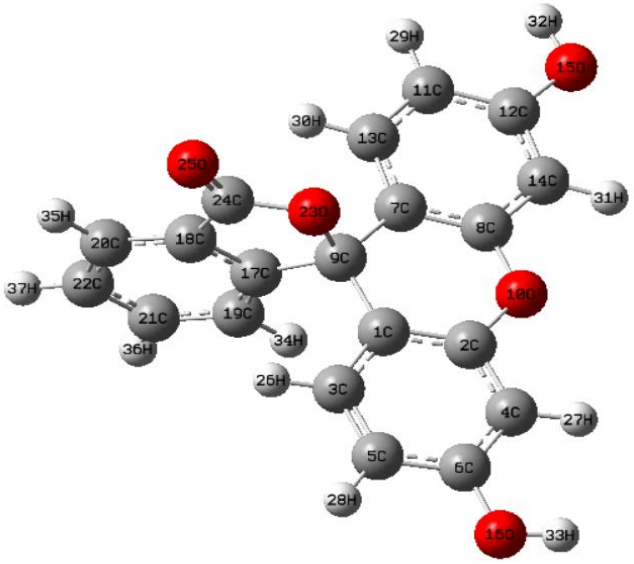

Figure 5. Structure of fluorescein in basic medium optimized by the DFT method B3LYP/6-31G(d,p).

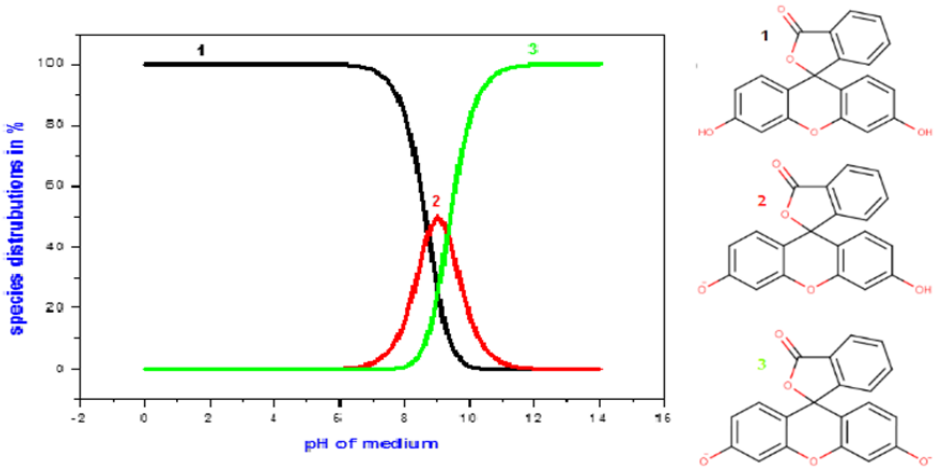

Figure 6. Distribution of different forms of fluorescein as a function of pH obtained from MARVISKETCH program.

The answer to this ambiguity was found by using the MARVINSKETCH software. The distribution of the protonated forms as a function of the pH shows that the desired shape can take place at a pH in the vicinity of 14 (Figure 6).

We proceeded by recalculating the same starting parameters, this time with fluorescein in basic medium.

Table 11. HOMO and LUMO energies and the energy differences between the two possible HOMO/LUMO combinations of DFT/B3LYP reagents, 6-31G(d,p).

Compound	*E* (eV)	HOMO (eV)	LUMO (eV)	Δ*E*(I) (eV)	Δ*E*(II) (eV)
Fluorescein (basic form)	–31144.6797	–4.2678	–1.2754	–1.6615	–6.1517
Tosyl chloride	–34823.7870	–7.4271	–2.6063		

$$\Delta E(\mathrm{I}) = E_{\mathrm{HOMO}}\ (\text{basic fluorescein}) - E_{\mathrm{LUMO}}\ (\text{tosyl chloride})$$

$$\Delta E(\mathrm{II}) = E_{\mathrm{HOMO}}\ (\text{tosyl chloride}) - E_{\mathrm{LUMO}}\ (\text{fluorescein})$$

The results from Table 11 show again that the $|E_{\mathrm{HOMO}}(\mathrm{fluo}) - E_{\mathrm{LUMO}}(\mathrm{TsCl})|$ are energetically weaker than the $|E_{\mathrm{HOMO}}(\mathrm{TsCl}) - E_{\mathrm{LUMO}}(\mathrm{fluo})|$ gaps, and therefore tosyl chloride behaves as an electrophile while fluorescein behaves like a nucleophile [36].

4.2.3.1. Theoretical analysis of reagents by global properties

Table 12 shows that the chemical potential μ of fluorescein ($\mu = -1.4962$ eV) is on a level of energy higher than that of tosyl chloride ($\mu = -2.4104$ eV), which implies that electron transfer takes place from fluorescein to tosyl chloride. We note this time that the value of the nucleophilic index of basic fluorescein is greater than that found for the neutral fluorescein, which shows the importance of the use of the base in the desired reaction ensuring its good approach. On the other hand, the results obtained show that, in basic medium, the nucleophilic index ($N = 4.8507$ eV) definitely higher than that of tosyl chloride ($N = 1.6915$ eV), which means that fluorescein is a nucleophile whereas tosyl chloride is an electrophile. The same conclusion can be drawn from the values of electrophilic indices.

Table 12. Electronic chemical potential μ, global hardness η, global electrophilicity ω, global nucleophilicity *N*, B3LYP DFT/6-31G(d,p).

Compound	*E* (eV)	μ (eV)	η (eV)	S(I) (eV)	ω (eV)	*N* (eV)
Neutral Fluorescein	–31171.2957	–2.3468	4.6937	0.1065	0.5867	2.9881
Basic fluorescein	–31144.6797	–1.4962	2.9924	0.1671	0.3741	4.8507
Tosyl chloride	–34823.7870	–2.4104	4.8208	0.1037	0.6026	1.6915

4.2.3.6. Prediction of local reactivity of reagents

• *Application of the Domingo polar model, using Fukui indices* f_k^+ *and* f_k^-

Table 13. Natural populations of fluorescein in basic medium and TsCl calculated by the method DFT/B3LYP 6-31G(d,p).

Natural populations					
Basic fluorescein			**Tosyl chloride**		
Atoms	***P*(*N*)**	***P*(*N*−1)**	**Atoms**	***P*(*N*)**	***P*(*N*+1)**
C_1	5.64353	5.65116	C_1	6.71022	6.69984
C_2	6.17145	6.06191	C_2	5.98321	6.05961
C_3	6.40879	6.32883	C_3	6.22547	6.23668
C_4	6.20284	6.20556	C_4	6.22523	6.23659
C_5	5.58542	5.57729	C_5	6.19874	6.25263
C_6	6.33306	6.24999	C_6	6.19892	6.25242
C_7	5.64352	5.65115	C_7	6.35084	6.36044
C_8	6.17143	6.06193	S_8	13.87483	14.03983
O_9	8.4831	8.46779	O_9	8.88976	8.99649
C_{10}	5.88407	5.89783	O_{10}	8.88977	8.99649
C_{11}	5.58541	5.57729			
C_{12}	6.33305	6.24999			
C_{13}	6.40879	6.32883			
C_{14}	6.20282	6.20554			
O_{15}	8.76686	8.75892			
C_{16}	5.23148	5.22608			
O_{17}	8.79047	8.78088			
C_{18}	6.12886	6.12296			
C_{19}	6.05703	6.07787			
C_{20}	6.22225	6.21693			
C_{21}	6.25137	6.24099			
C_{22}	6.23176	6.22804			
C_{23}	6.24311	6.23744			
O_{24}	8.72036	8.5849			
O_{25}	8.72036	8.58489			

From natural populations, we calculated local Fukui indices of the reagents used to synthesize the desired product.

Table 14. Fukui indices (f_k^+ and f_k^-) and local electrophilicity values ω_k for reactive TsCl atoms and N_k local nucleophilicity for reactive basic fluorescein atoms calculated by NPA population analysis.

Local indices NPA					
Basic fluorescein			**Tosyl chloride**		
Atoms	f^-	N_k	**Atoms**	f^+	ω_k
C_1	–0.008	–0.037	C_1	–0.010	–0.006
C_2	0.110	0.531	C_2	0.076	0.046
C_3	0.080	0.388	C_3	0.011	0.007
C_4	–0.003	–0.013	C_4	0.011	0.007
C_5	0.008	0.039	C_5	0.054	0.032
C_6	0.083	0.403	C_6	0.053	0.032
C_7	–0.008	0.037	C_7	0.010	0.006
C_8	0.110	0.531	S_8	0.165	0.099
O_9	0.015	0.074	O_9	0.107	0.064
C_{10}	–0.014	0.067	O_{10}	0.107	0.064
C_{11}	0.008	0.039			
C_{12}	0.083	0.403			
C_{13}	0.080	0.388			
C_{14}	–0.003	0.013			
O_{15}	0.008	0.039			
C_{16}	0.005	0.026			
O_{17}	0.010	0.047			
C_{18}	0.006	0.029			
C_{19}	–0.021	–0.101			
C_{20}	0.005	0.026			
C_{21}	0.010	0.050			
C_{22}	0.004	0.018			
C_{23}	0.006	0.028			
O_{24}	0.135	0.657			
O_{25}	0.135	0.657			

This time, the local N_k nucleophilic indices for the fluorescein reactive atoms in the basic medium and the local electrophilic indices ω_k for the tosyl chloride atoms show that the most favored interaction takes place between the most electrophilic site (characterized by the highest value of ω_k) of the electrophilic molecule and the most nucleophilic site (characterized by the highest N_k value) of the nucleophilic molecule. Consequently, the formation of the O_{24}–S_8 and O_{25}–S_8 bonds, experimentally desired, is correctly predicted by the Domingo polar model.

• *Application of the Gazquez–Mendez rule using condensed local softness (Sk^+ and Sk^-)*

According to the Gazquez–Mendez rule, "Two chemical species interact through atoms with similar or similar softness". The local softness values Sk^- for the reactive atoms of fluorescein and local softness Sk^+ for the reactive atoms of tosyl chloride, calculated with the NPA population analysis, are given in Table 15 [38].

Table 15. Fukui indices (f_k^+ and f_k^-) and Sk^- local softness values for reactive fluorescein and Sk^+ local softness atoms for tosyl chloride reactive atoms, calculated by NPA populations.

Local indices NPA					
Basic fluorescein			**Tosyl chloride**		
Atoms	f_k^-	Sk^-	**Atoms**	f_k^+	Sk^+
C_1	–0.008	–0.001	C_1	–0.010	–0.001
C_2	0.110	0.018	C_2	0.076	0.008
C_3	0.080	0.013	C_3	0.011	0.001
C_4	–0.003	0.000	C_4	0.011	0.001
C_5	0.008	0.001	C_5	0.054	0.006
C_6	0.083	0.014	C_6	0.053	0.006
C_7	–0.008	–0.001	C_7	0.010	0.001
C_8	0.110	0.018	S_8	0.165	0.017
O_9	0.015	0.003	O_9	0.107	0.011
C_{10}	–0.014	–0.002	O_{10}	0.107	0.011
C_{11}	0.008	0.001			
C_{12}	0.083	0.014			
C_{13}	0.080	0.013			
C_{14}	–0.003	0.000			
O_{15}	0.008	0.001			
C_{16}	0.005	0.001			

Local indices NPA					
Basic fluorescein			**Tosyl chloride**		
Atoms	f_k^-	Sk^-	**Atoms**	f_k^+	Sk^+
O_{17}	0.010	0.002			
C_{18}	0.006	0.001			
C_{19}	–0.021	–0.003			
C_{20}	0.005	0.001			
C_{21}	0.010	0.002			
C_{22}	0.004	0.001			
C_{23}	0.006	0.001			
O_{24}	0.135	0.023			
O_{25}	0.135	0.023			

With $Sk^+ = S \cdot f_k^+$ ($S = 1/2 \cdot \eta = 0.1037$ eV^{-1}), $Sk^- = S \cdot f_k^-$ ($S = 0.1671$ eV^{-1}).

Table 15 also show that the most favored interactions takes place between the atom S_8 of tosyl chloride and the O_{24} and O_{25} fluorescein (neighboring local softness), which is in good agreement with the experimentally results.

5. Application against corrosion in hydrochloric acid solution

5.1. Stability in acid environment

In order to find available information about the stability of NAR1 inhibitor in acidic solution, the infrared analysis has been investigated before and after contact with hydrochloric acid solution.

From infrared analysis Figure 7 and Table 16, the result obtained explains the stability behavior of NAR1 inhibitor in acidic medium. Therefore, any transformation of organic function in inhibitor molecule that can be justified the choice of acid environment as corrosion medium.

Table 16. Bands assignments (cm^{-1}) of NAR1 in the IR spectrum.

Assignment	Frequencies (cm^{-1})
ν(O–H)	3800–3600
ν(=C–H) aromatic	3200–2800
ν(C=O)	1700–1550
ν(C–O)	1500–1080
ν(S=O)	1235–1092

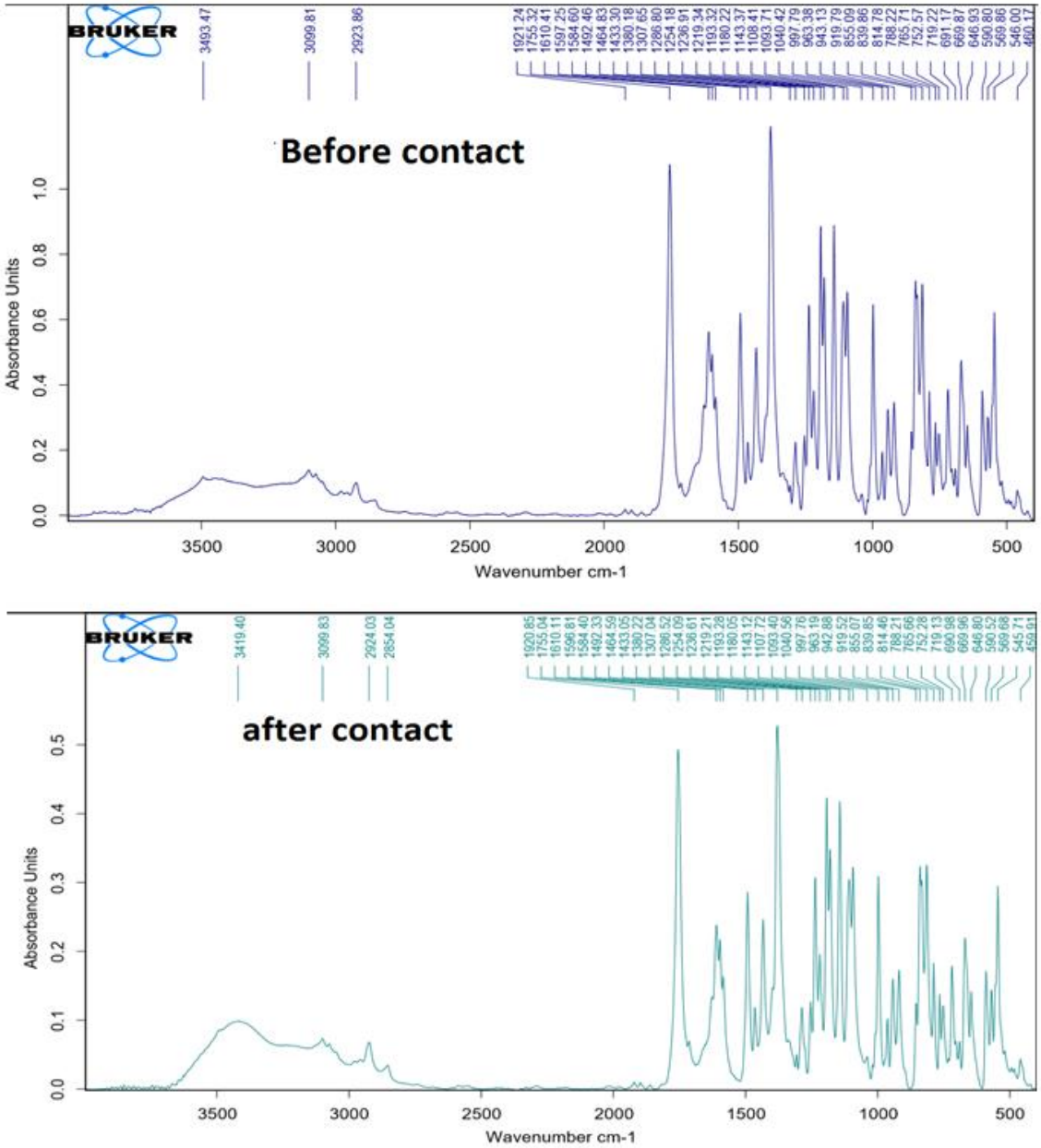

Figure 7. IR spectrums of NAR1 inhibitor before and after contact in acid solution.

5.2 Absorbance difference measurements

The absorbance difference measurement is a simple technique which applied using a UV/Visible spectrophotometer (UV-6300PC, Double Beam Spectrophotometer). The mild steel samples are immersed in these solutions and placed in thermostated water during 6 h at 298 K. Then, the absorbance measurements ($A°$) and (A) are taken before and after immersion at a wavelength of 300–310 nm.

The difference between ($A°$) and (A) was recorded as the absorbance difference of the corrodent in each case. All the reported readings are average of five experimental readings.

The inhibition efficiency of NAR1 inhibitor was calculated using the following equation [39]:

$$IE(\%) = \frac{A^\circ - A}{A^\circ} \cdot 100$$

Where ($A°$) and (A) are absorbance for mild steel with and without NAR1 in 1 M HCl medium at 298 K.

Table 17. Inhibition efficiency and absorbance difference for NAR1 in 1 M HCl solution at 298 K after 6 h of immersion.

Medium	Concentration (ppm)	Absorbance difference	Efficiency (%)
1 M HCl	–	0.558	–
NAR1	1	0.039	93.0
	0.75	0.067	88.0
	0.50	0.078	86.0
	0.25	0.134	76.0

The Table 17 shows the percentage of inhibition effect of mild steel at various concentrations of fluorescein in acidic media at 298 K from absorbance difference measurements. The result obtained from this technique, indicate that the inhibition efficiency increases slightly with inhibitor concentrations to achieve 93% at 1 ppm. This inhibition behavior of synthetic product can be reported to the ability of this compound to form protective film onto the steel surface, through the vacant d-orbital of iron and delocalized π electrons on the length of inhibitor molecule [40].

5.3. Surface analysis

The surface analysis result of mild steel in the presence and absence of NAR1 inhibitor after immersion throughout 6 hour at 298 K was investigated to point out the percentage of atoms absorbable on the surface of working electrode [41–45]. SEM micrographs are presented in Figure 8. The surface of mild steel after immersion in 1 M HCl is too undamaged compared with the mild steel after immersed in 1 ppm of NAR1 inhibitor due to the formation of a heterogeneous protective film [46] (Figure 8C).

The EDX technique have been used in order to identify the chemical composition of working electrode and the component adsorbed onto the mild steel surface before and after immersed in different solution with and without NAR1 inhibitor at optimum concentration.

The EDX spectra showing in Figure 9 and the percentage atomic of various atoms adsorbed on the surface of working electrode are regrouped in Table 18. It's clear from the difference between the values of percentage atomic for mild steel after immersed in uninhibited and inhibited solution, that the fluorescein inhibitor protects the mild steel

against corrosive medium. The obtained results are in good agreement with those obtained recently [47].

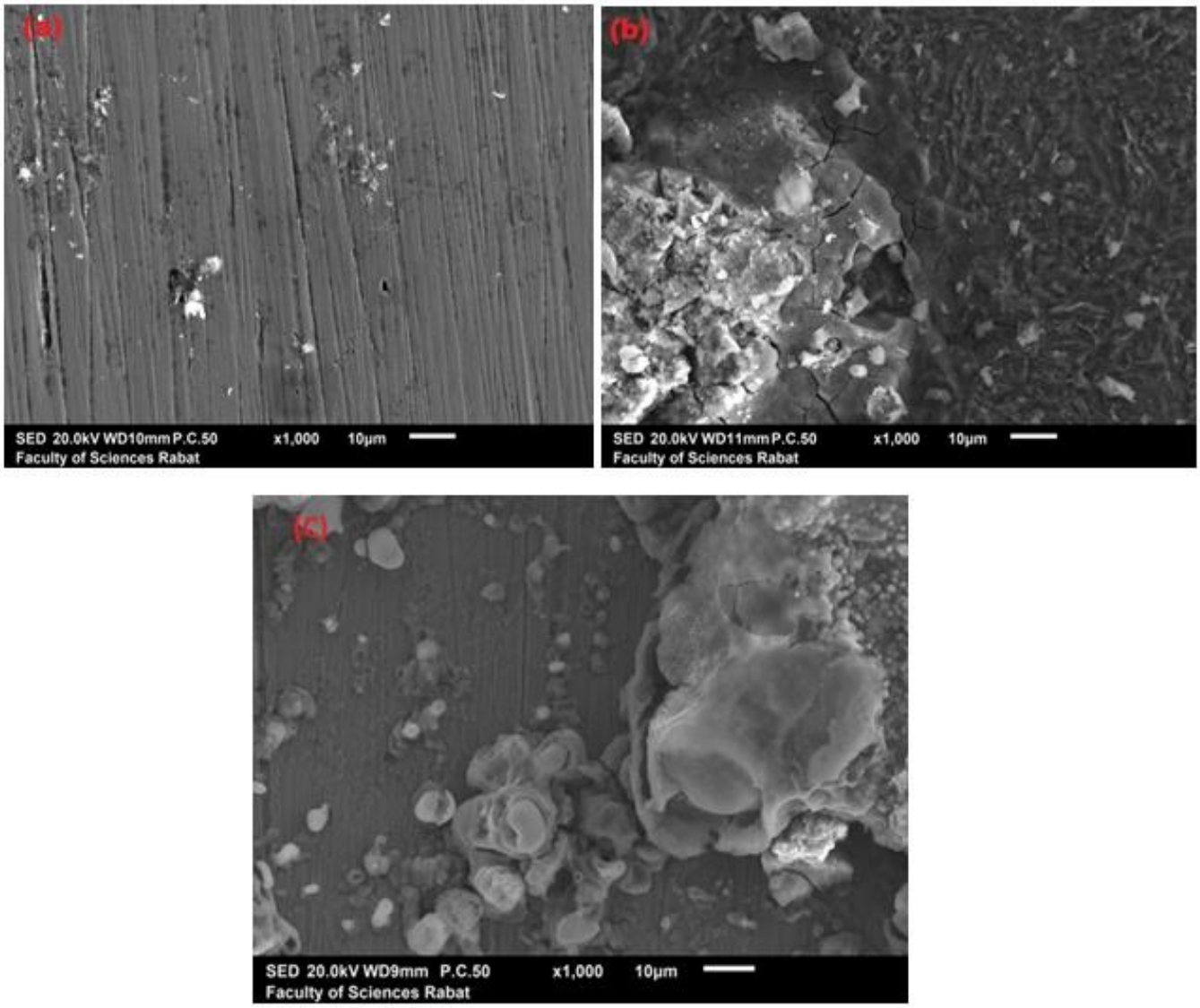

Figure 8. SEM micrographs of mild steel before immersion (a) after 6 h immersion in 1 M of HCl (b) after immersion in 1 ppm of NAR1 inhibitor (C)

Table 18. Percentage atomic contents of elements obtained from EDX spectra.

Elements adsorbed	Fe	C	Cr	Mn	Cl	S	O
Mild steel	96.01	2.14	0.65	0.97	–	–	0.23
Mild steel in 1 M of HCl	83.91	4.25	0.37	0.50	2.97	–	8.00
Mild steel in 1 ppm of NAR1	74.89	3.88	0.24	0.97	0.49	2.08	17.45

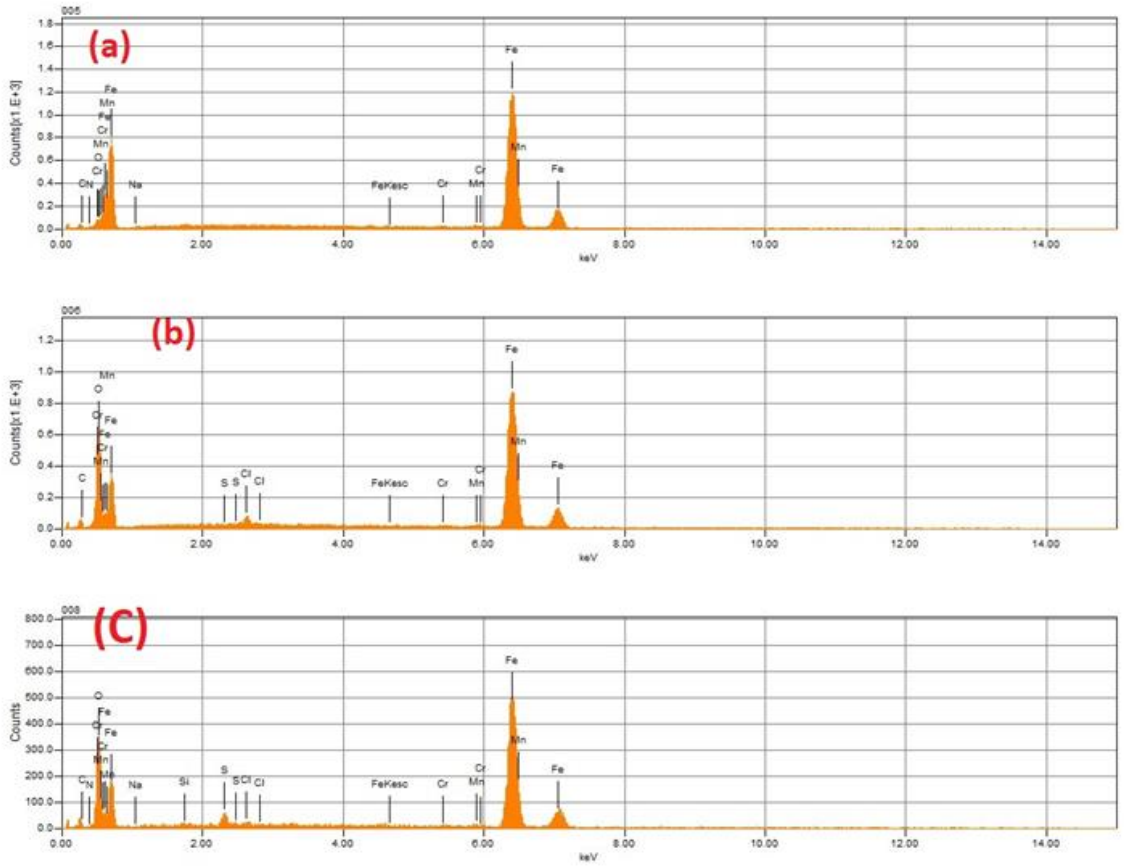

Figure 9. EDX spectra of mild steel before immersion (a) after 6 h immersion in 1 M of HCl (b) after immersion in 1 ppm of NAR1 inhibitor (C).

Conclusion

In conclusion, this method provides general and convenient access to a wide range of fluorescein derivatives starting from the appropriate fluorescein. The nucleophilic substitution of fluorescein with 4-methyl-benzenesulfonyl chloride occurred under very mild conditions and led to the 3-oxo-3*H*-spiro[isobenzofuran-1,9′-xanthene]-3′,6′-diyl bis(3-methylbenzenesulfonate) in high yield. The structure of the synthesized product was analyzed by MS, Infrared, ^{13}C NMR and ^{1}H NMR. This reaction has been studied using MARVINSKETCH in order to find range of pH in the major form of fluorescein in basic medium and Gaussian 09 program within the DFT calculations at the B3LYP/6-31(d,p) computational level. The analysis of the electrophilic and nucleophilic Parr functions of reagents and an exploration of the values of the energy E and the relative energy ΔE of this reaction indicates that it takes place through a two-step mechanism. The exothermic character of this reaction makes the formation of the new product 3 irreversible, thermodynamically and kinetically favored in good agreement with experimental result. Then, the anti-corrosion activities of the synthetic product has been studied using difference absorbance method, the result reflect the higher inhibition behavior against corrosion of mild steel in acidic medium.

Acknowledgements

We thank the CNRST for financial support of this work (PROTARS D13/03, Morocco).

References

1. K. Dioukhane, A. Alami, Y. Aouine, M. El Omari, L. El Ammari, M. Saadi, A. Assani and R. Ouarsal, Synthesis, Crystal Structure and IR Spectrum studies of 2-(4-Methyl-2-phenyl-4,5-dihydro-oxazol-4-ylmethyl)- isoindole-1,3-dione, *Mediterr. J. Chem.*, 2019, **9**, no. 2, 116–124. doi: 10.13171/mjc92190916245aa
2. M.C. Bagley, K.D. Chapaneri, W. Dale, X. Xiong and J. Bower, One-Pot Multistep Bohlmann−Rahtz Heteroannulation Reactions: Synthesis of Dimethyl Sulfomycinamate, *J. Org. Chem.*, 2005, **70**, 1389–1399. doi: 10.1021/jo048106q
3. Y. Wang, H. Chen, C. Li and P. Wu, Octachloro-fluorescein: Synthesis and photosensitizer performance evaluation, *Dyes Pigm.*, 2019, **170**, 107635. doi: 10.1016/j.dyepig.2019.107635
4. V.S. Vinutha, N. Badiadka and K.S. Balladka, *N*-(4-Nitrophenyl)-2-{2-[3-(4-chlorophenyl)-5-[4-(propan-2-yl)phenyl]-4,5-dihydro-1*H*-pyrazol-1-yl]-4-oxo-4,5-dihydro-1,3-thiazol-5-yl}acetamide, *Molbank*, 2017, **M943**. doi: 10.3390/M943
5. L. Rinaldi, K. Martina, F. Baricco, L. Rotolo and G. Cravotto, Solvent-Free Copper-Catalyzed Azide-Alkyne Cycloaddition under Mechanochemical Activation, *Molecules*, 2015, **20**, 2837–2849. doi: 10.3390/molecules20022837
6. M.S. Singh, S. Chowdhury and S. Koley, Advances of azide-alkyne cycloaddition-click chemistry over the recent decade, *Tetrahedron*, 2016, **72**, 5257–5283. doi: 10.1016/j.tet.2016.07.044
7. T.Y. Zhang, C.J. Zheng, J. Wu, L.P. Sun and H.R. Piao, Synthesis of novel dihydrotriazine derivatives bearing 1,3-diaryl pyrazole moieties as potential antibacterial agents, *Bioorg. Med. Chem. Lett.*, 2019, **29**, 1079–1084. doi: 10.1016/j.bmcl.2019.02.033
8. A.T. Taher, M.T.M. Sarg, N.R. El-Sayed Ali and N.H. Elnagdi, Design, synthesis, modeling studies and biological screening of novel pyrazole derivatives as potential analgesic and anti-inflammatory agents, *Bioorg. Chem.*, 2019, **89**, 103023. doi: 10.1016/j.bioorg.2019.103023
9. F. Ran, Y. Liu, D. Zhang, M. Liu and G. Zhao, Discovery of novel pyrazole derivatives as potential anticancer agents in MCL, *Bioorg. Med. Chem. Lett.*, 2019, **29**, 1060–1064. doi: 10.1016/j.bmcl.2019.03.005
10. J.D. Moore, K.T. Sprott and P.R. Hanson, Conformationally Constrained α-Boc-Aminophosphonates *via* Transition Metal-Catalyzed/Curtius Rearrangement Strategies, *J. Org. Chem.*, 2002, **67**, 8123–8129. doi: 10.1021/jo0262208

11. C.D. Sant'ana, D.L. Menaldo, T.R. Costa, H. Godoy, V.D. Muller, V.H. Aquino, S. Albuquerque, S.V. Sampaio, M.C. Monteiro, R.G. Stábeli and A.M. Soares, RETRACTED: Antiviral and antiparasite properties of an l-amino acid oxidase from the Snake *Bothrops jararaca*: Cloning and identification of a complete cDNA sequence, *Biochem. Pharmacol.*, 2008; **76**, 279–288. doi: 10.1016/j.bcp.2008.05.003
12. G.F.S. Fernandes, C.M. Chin and J.L. Santos, Advances in Drug Discovery of New Antitubercular Multidrug-Resistant Compounds, *Pharmaceuticals*, 2017, **10**, 51. doi: 10.3390/ph10020051
13. A. Zhang, J. Zhou, K. Tao, T. Hou and H. Jin, Design, synthesis and antifungal evaluation of novel pyrazole carboxamides with diarylamines scaffold as potent succinate dehydrogenase inhibitors, *Bioorg. Med. Chem. Lett.*, 2018, **28**, 3042–3045. doi: 10.1016/j.bmcl.2018.08.001
14. M. Zhang, Q. Chen and G.-F. Yang, A review on recent developments of indole-containing antiviral agents, *Eur. J. Med. Chem.*, 2015, **89**, 421–441. doi: 10.1016/j.ejmech.2014.10.065
15. G.D. Joly and E.N. Jacobsen, Thiourea-Catalyzed Enantioselective Hydrophosphonylation of Imines: Practical Access to Enantiomerically Enriched α-Amino Phosphonic Acids, *J. Am. Chem. Soc.*, 2004, **126**, 4102–4103. doi: 10.1021/ja0494398
16. K.C. Prakasha, G.M. Raghavendra, R. Harisha and G.D. Channe, *Int. J. Pharm. Pharm. Sci.*, 2011, **3**, 120–125.
17. M. Monici, Cell and tissue autofluorescence research and diagnostic applications, *Biotechnol. Annu. Rev.*, 2005, **11**, 227–256. doi: 10.1016/S1387-2656(05)11007-2
18. R.P. Haugland, M.T.Z. Spence, I.D. Johnson and A. Basey, *The handbook: a guide to fluorescent probes and labeling technologies*, 2005, Molecular Probes, Eugene Or.
19. S. Tyagi and F.R. Kramer, Molecular Beacons: Probes that Fluoresce upon Hybridization, *Nat. Biotechnol.*, 1996, **14**, 303–308. doi: 10.1038/nbt0396-303
20. D. Sahoo, V. Narayanaswami, C.M. Kay and R.O. Ryan, Pyrene Excimer Fluorescence: A Spatially Sensitive Probe To Monitor Lipid-Induced Helical Rearrangement of Apolipophorin III, *Biochemistry*, 2000, **39**, 6594–6601. doi: 10.1021/bi992609m
21. M.K. Smalley and S.K. Silvermann, Fluorescence of covalently attached pyrene as a general RNA folding probe, *Nucleic Acids Res.*, 2006, **34**, 152–166. doi: 10.1093/nar/gkj420
22. F. Sussmeier and H. Langhals, Novel Fluorescence Labels: The Synthesis of Perylene-3,4,9-tricarboxylic Imides, *Eur. J. Org. Chem.* 2001, 607–610. doi: 10.1002/1099-0690(200102)2001%3A3<607%3A%3AAID-EJOC607>3.0.CO%3B2-N
23. S.G. Schulman, R.M. Threatte, A.C. Capomacchia and W.L. Paul, Fluorescence of 6-Methoxyquinoline, Quinine, and Quinidine in Aqueous Media, *J. Pharm. Sci.*, 1974, **63**, 876–880. doi: 10.1002/jps.2600630615
24. S. Jayaraman and A.S. Verkman, *Biophys. Chem.*, 2000, **85**, 49–57. doi: 10.1016/S0301-4622(00)00146-0

25. A. Loudet and K. Burgess, BODIPY Dyes and Their Derivatives: Syntheses and Spectroscopic Properties, *Chem. Rev.*, 2007, **107**, 4891–4932. doi: 10.1021/cr078381n
26. R.B. Mujumdar, L.A. Ernst, S.R. Mujumdar, C.J. Lewis and A.S. Waggoner, Cyanine dye labeling reagents: Sulfoindocyanine succinimidyl esters, *Bioconjugate Chem.*, 1993, **4**, 105–111. doi: 10.1021/bc00020a001
27. V. Buchmann, K.D. Weston and M. Sauer, Spectroscopic Study and Evaluation of Red-Absorbing Fluorescent Dyes, *Bioconjugate Chem.*, 2003, **14**, 195–204. doi: 10.1021/bc025600x
28. G. Cosa, K.S. Focsaneanu, J.R.N. Mclean, J.P. McNamee and J.C. Scaiano, Photophysical Properties of Fluorescent DNA-dyes Bound to Single- and Double-stranded DNA in Aqueous Buffered Solution, *Photochem. Photobiol.*, 2001, **73**, 585–599. doi: 10.1562/0031-8655(2001)0730585PPOFDD2.0.CO2
29. S. Erbas-Cakmak, D.A. Leigh, C.T. McTernan and A.L. Nussbaumer, Artificial Molecular Machines, *Chem. Rev.*, 2015, **115**, 10081–10206. doi: 10.1021/acs.chemrev.5b00146
30. Y. Na, Recent cancer drug development with xanthone structures, *J. Pharm. Pharmacol.*, 2009, **61**, 707–712. doi: 10.1211/jpp.61.06.0002
31. M.E. Sousa and M.M.M. Pinto, Synthesis of Xanthones: An Overview, *Curr. Med. Chem.*, 2005, **12**, 2447–2479. doi: 10.2174/092986705774370736
32. A. Meijere, Adolf von Baeyer: Winner of the Nobel Prize for Chemistry 1905, *Chem. Int. Ed.*, 2005, **44**, 7836–7840. doi: 10.1002/anie.200503351
33. M. Jabri, M. Lakrat, E. Mejdoubi, B. Hammouti, H. Demnati and A. Asehraou, Synthesis and Antibacterial Study of New Microporous Zinc Phosphate Bioceramics, *Moroccan J. Chem.*, 2019, **7**, no. 4, 739–747.
34. M.O. Abdulazeez, A.K. Oyebamiji and B. Semire, DFT-QSAR studies on corrosion inhibition efficiency of derivatives of thiadiazole, oxadiazole and triazole, *Int. J. Corros. Scale Inhib*, 2016, **5**, no. 3, 248–262. doi: 10.17675/2305-6894-2016-5-3-5
35. A. El Yaktini, A. Lachiri, M. El Faydy, F. Benhiba, H. Zarrok, M. El Azzouzi, M. Zertoubi, M. Azzi, B. Lakhrissi and A. Zarrouk, *Int. J. Corros. Scale Inhib.*, 2018, **7**, no. 4, 609–632. doi: 10.17675/2305-6894-2018-7-4-9
36. S. Hadisaputra, A.A. Purwoko, I. Ilhamsyah, S. Hamdiani, D. Suhendra, N. Nuryono and B. Bundjali, *Int. J. Corros. Scale Inhib.*, 2018, **7**, no. 4, 633–647. doi: 10.17675/2305-6894-2018-7-4-10
37. L.R. Domingo and P. Pérez, The nucleophilicity *N* index in organic chemistry, Org. *Biomol. Chem.*, 2011, **9**, 7168–7175. doi: 10.1039/C1OB05856H
38. P. Pérez, L.R. Domingo, M. Duque-Noreňa and E.A. Chamorro, A condensed-to-atom nucleophilicity index. An application to the director effects on the electrophilic aromatic substitutions, *J. Mol. Struct.: THEOCHEM*, 2009, **895**, 86–91. doi: 10.1016/j.theochem.2008.10.014

39. A.I. Onen, B.T. Nwufo, E. Ebenso and R.M. Hlophe, Titanium (IV) Oxide as Corrosion Inhibitor for Aluminium and Mild Steel in Acidic Medium, *Int. J. Electrochem. Sci.*, 2010, **5**, 1563–1573.
40. A. Ezeibe, E. Nleonu and A. Ahumonye, *Int. J. Sci. Eng. Res.*, 2019, **7**, no. 2, 133–136.
41. F. El-Hajjaji, M. Messali, M.V. Martínez de Yuso, E. Rodríguez-Castellón, S. Almutairi, T.J. Bandosz and M. Algarra, Effect of 1-(3-phenoxypropyl) pyridazin-1-ium bromide on steel corrosion inhibition in acidic medium, *J. Colloid Interface Sci.*, 2019, **541**, 418–424. doi: 10.1016/j.jcis.2019.01.113
42. F. El-Hajjaji, M. Messali, A. Aljuhani, M.R. Aouad, B. Hammouti, M.E. Belghiti, D.S. Chauhan and M.A. Quraishi, *J. Mol. Liq.*, 2018, **249**, 997–1008. doi: 10.1016/j.molliq.2017.11.111
43. R. Salim, E. Ech-chihbi, H. Oudda, F. El Hajjaji, M. Taleb and S. Jodeh, A review on the assessment of Imidazo1,2-apyridines As corrosion inhibitor of metals, *J. Bio- Tribo Corros.*, 2019, **5**, 14. doi: 10.1007/s40735-018-0207-3
44. El. Ech chihbi, A. Nahlé, R. Salim, H. Oudda, F. El Hajjaji, F. El Kalai, A. El Aatiaoui and M. Taleb, An Investigation into Quantum Chemistry and Experimental Evaluation of Imidazopyridine Derivatives as Corrosion Inhibitors for C-Steel in Acidic Media, *J. Bio- Tribo Corros.*, 2019, **5**, 24. doi: 10.1007/s40735-019-0217-9
45. F. El Hajjaji, F. Abrigach, O. Hamed, A.R. Hasan, M. Taleb, S. Jodeh, E. Rodríguez-Castellón, M.V.M. Yuso and M. Algarra, Corrosion Resistance of Mild Steel Coated with Orgainc Material Containing Pyrazol Moiety, *Coatings*, 2018, **8**, 330. doi: 10.3390/coatings8100330
46. A. El Janati, Y. Kandri Rodi, M. Mokhtari, I. Abdel-Rahman, I. Alaoui, F.Ouazzani Chahdi, Y. Ouzidan, H. Steli, H. Elmsellem and B. Hammouti, *Int. J. Corros. Scale Inhib.*, 2019, **8**, no. 3**,** 702–716. doi: 10.17675/2305-6894-2019-8-3-17
47. N. Arrousse, E. Mabrouk, B. Hammouti, F. El Hajjaji, Z. Rais and M. Taleb, New strategy of synthesis, characterization, theoretical study and inhibition effect on mild steel corrosion in acidic solution, *Mediterr. J. Chem.*, 2020, **10**, no. 5, 477–491. doi: 10.13171/mjc10502005151417feh

♦ ♦ ♦